MATHEMATICAL FRAMEWORK FOR SYNTHETIC DATA GENERATION IN ELECTRIC MOTOR PREDICTIVE ANALYTICS

Sergey E. Simonov,
Moscow Technical University of Communications and Informatics, Moscow, Russia,
s.e.simonov@mtuci.ru

Marina V. Yashina,
Moscow Technical University of Communications and Informatics, Moscow, Russia

Sergey Y. Kazantsev,
Moscow Technical University of Communications and Informatics, Moscow, Russia

Sergey P. Degtyarev,
Moscow Technical University of Communications and Informatics, Moscow, Russia,
s.p.degtyaryov@mtuci.ru

Kirill S. Shishkin,
Moscow Technical University of Communications and Informatics, Moscow, Russia,
k.s.shishkin@mtuci.ru

Mikhail G. Gorodnichev,
Moscow Technical University of Communications and Informatics, Moscow, Russia,
m.g.gorodnichev@mtuci.ru

DOI: 10.36724/2072-8735-2026-20-34-60-74

Manuscript received 17 January 2026;
Accepted 21 March 2026

Keywords: *mathematical software, electric motor, synthetic data gen-eration, interrelation of vibration, temperature and electro-magnetic component*

This paper addresses the problem of developing a gen-eralized mathematical model of an electric motor that ac-counts for the coupled influence of electromagnetic, me-chanical, vibrational, and thermal processes. The objective of the study is to construct a compact analytical model suit-able for predictive analytics and synthetic data generation for training intelligent diagnostic systems. The research methodology is based on the formulation of a system of or-dinary differential equations describing the dynamics of current, angular velocity, vibration displacement, and tem-perature, with explicit consideration of interactions between different physical subsystems. The model incorporates the temperature dependence of electrical parameters, the influence of vibrations on friction and heat generation, as well as feedback mechanisms between subsystems. A theoretical analysis of the model is performed, including proofs of local and global solvability and the derivation of a priori estimates of solutions. Numerical experiments were conducted by simulating motor operation with subsequent addition of noise to emulate real measurement conditions. The results reveal characteristic patterns of transient processes, including the effect of vibrations on dynamic stabilization and temperature rise. The results can be applied in the development of digital twins, predictive maintenance systems, and synthetic dataset generation. The proposed model provides a balance between physical interpretability and computational efficiency, making it suitable for real-time applications.

Information about authors:

Sergey E. Simonov, *Moscow Technical University of Communications and Informatics, Senior lecturer of the Department of Mathematical Cybernetics and Information Technology, Post-graduate student, Moscow, Russia. ORCID: 0000-0003-3391-8064*

Marina V. Yashina, *Moscow Technical University of Communications and Informatics, Principal lecturer of the Department of Mathematical Cybernetics and Information Technology, Doctor of Sciences in Engineering, Moscow, Russia. ORCID: 0000-0001-8810-918X*

Sergey Y. Kazantsev, *Moscow Technical University of Communications and Informatics, Professor of the Department of Guiding Telecommuni-cation Environments, Doctor of Sciences in Physical and Mathematical Sciences, Moscow, Russia. ORCID: 0000-0002-0189-5286*

Sergey P. Degtyarev, *Moscow Technical University of Communications and Informatics, Professor of the Department of Mathematical Cyber-netics and Information Technology, Doctor of Sciences in Physical and Mathematical Sciences, Moscow, Russia. ORCID: 0000-0003-1295-5405*

Kirill S. Shishkin, *Moscow Technical University of Communications and Informatics, Assistant lecturer of the Department of Mathematical Cybernetics and Information Technology, Post-graduate student, Moscow, Russia. ORCID: 0009-0001-9076-1756*

Mikhail G. Gorodnichev, *Moscow Technical University of Communications and Informatics, Head of the Department of Mathematical Cybernetics and Information Technology, PhD in Engineering, Moscow, Russia. ORCID: 0000-0003-1739-9831*

Для цитирования:
Симонов С.Е., Яшина М.В., Казанцев С.С., Дегтярёв С.П., Шишкин К.С., Городничев М.Г. Математическое обеспечение генерации синтетических данных для предиктивной аналитики электродвигателей // T-Comm: Телекоммуникации и транспорт. 2026. Том 20. №4. С. 60-74.

For citation:
S.E. Simonov, M.V. Yashina, S.Y. Kazantsev, S.P. Degtyarev, K.S. Shishkin, M. G. Gorodnichev, “Mathematical framework for synthetic data generation in electric motor predictive analytics,” *T-Comm*, 2026, vol. 20, no. 4, pp. 60-74.

Introduction

Electric motors are critical components of modern industrial equipment, transportation, and energy systems. Their reliability directly determines the efficiency of technological processes and the economic performance of operations. Traditional diagnostic methods rely on the analysis of electrical, mechanical, vibrational, and thermal parameters, but these are typically considered in isolation, which limits the comprehensiveness of condition assessment. With the advancement of remote monitoring systems and predictive maintenance, the development of integrated models that combine various physical processes into a unified mathematical framework has become particularly significant. Such a model enables the generation of reliable synthetic data, expanding training datasets for intelligent diagnostic algorithms, thereby improving the accuracy of failure prediction and optimizing the operational modes of electric motors.

Existing motor models primarily focus on describing individual physical processes: electrical, mechanical, vibrational, or thermal. This fragmented approach restricts the potential for comprehensive diagnostics and predictive analytics, as real-world motor operation is governed by the interplay of these processes. In the context of advancing intelligent monitoring systems, there is a need for a generalized mathematical model that accounts for electrical, mechanical, vibrational, and thermal phenomena.

The objective of this study is to develop a generalized mathematical model of an electric motor that integrates electrical, mechanical, vibrational, and thermal processes.

The generalized mathematical model of an electric motor serves as a tool for design and optimization, enables the creation of digital twins, reduces the costs of physical testing, and supports the prediction of service life and reliability assessment under various operating conditions, including emergency scenarios. Such a model can be applied in the development and tuning of control systems, for educational purposes in training engineers, and for integration with IoT systems and big data, facilitating comprehensive monitoring and enhancing the operational efficiency of electric motors across various types and ratings.

1. Related work

Research on fault diagnosis of induction motors (IMs) has long been based on the fact that many mechanical defects leave characteristic signatures in electrical quantities, primarily in the stator current [1]. One of the key research directions is physics-based current modeling, which links the dynamics of bearing defects to measurable current components. In several studies, stator current models for detecting rolling bearing faults have been developed using magnetic equivalent circuits (MECs), demonstrating how fault-induced air-gap magnetic field modulations are transferred into diagnostic current components without the need for full transient finite-element modeling [2]. Similar MEC-based approaches have also been applied to other types of faults, such as broken rotor bars, where interpolation functions are used to describe variations in electromagnetic parameters caused by the defect [3]. In parallel, state-space models have been developed that allow asymmetries, such as static eccentricity, to be taken into account and their impact on electrical signals to be analyzed dynamically [4]. More general dynamic models of induction motors, focused on the analysis of electromechanical interactions, provide a foundation for understanding how mechanical disturbances manifest themselves in electrical variables [5].

A second important research direction is related to coupled electromagnetic-dynamic modeling, which aims at a more realistic reproduction of bearing fault mechanisms, including unbalanced magnetic pull (UMP) and its interaction with rotor motion and the bearing assembly [6]. In a number of studies, coupled electromagnetic-dynamic models of induction motors with bearing defects have been developed with explicit consideration of UMP, and the influence of this interaction on diagnostic features in measured signals, including stator current, has been analyzed [7]. Subsequent works have proposed systematic electromagnetic–dynamic modeling methods aimed at detecting bearing faults via stator current and have emphasized the necessity of simultaneously accounting for mechanical motion and electromagnetic asymmetry in order to obtain realistic fault signatures [8]. Complementing these approaches, dedicated studies have focused on the calculation and analysis of unbalanced magnetic pull under air-gap eccentricity faults, which helps to explain the origin of radial forces that excite vibrations and accelerate component degradation [9]. To integrate different physical subsystems and simulation environments, co-simulation approaches have also been employed, for example by coupling an induction machine model with a detailed radial ball bearing model to analyze mechanical defects within an electromechanical framework [10]. Taken together, these studies indicate that accurate reproduction of bearing fault manifestations generally requires multiphysics coupling of the electromagnetic domain, rotor dynamics, and bearing mechanics [7-10].

Alongside fault modeling, the field of digital twins and real-time multiphysics models for electrical machines has been actively developing. Particular attention is paid to thermal processes, as temperature significantly affects electrical parameters, losses, and overall reliability. Digital twin–based predictive thermal models have been proposed for stator temperature monitoring in induction motors, targeting online estimation and forecasting capabilities [11]. In a broader multiphysics context, dynamic electromagnetic–thermal mapping approaches have been developed for motor digital twins, providing computational efficiency and enabling real-time operation [12]. In addition, methods that integrate physical modeling with data-driven techniques have gained increasing attention, including digital twins based on physics-informed deep operator networks, which demonstrate the potential to reproduce complex multiphysics relationships with reduced computational cost [13]. Although many digital twin studies primarily focus on thermal and operational monitoring, they highlight the need for fast and physically interpretable models suitable for online applications [11-13, 14].

A closely related direction is high-fidelity multiphysics modeling for synthetic fault data generation. Comprehensive multiphysics models of induction motors have been developed to generate synthetic datasets under various bearing fault scenarios, which is particularly important for training and validating diagnostic algorithms [15]. Similar high-fidelity approaches have also been demonstrated for permanent magnet synchronous motors, where detailed multiphysics models are used to generate fault-related data [16]. At the same time, analytical models remain relevant as a basis for fast computation and design-oriented studies, for example for multiphase machines, where a balance

between accuracy and computational efficiency is required [17]. Despite their high realism, such models are often too computationally demanding for rapid parametric analysis and, in particular, for real-time applications [18].

The literature analysis reveals a clear trade-off between detailed multiphysics and co-simulation models, which provide high physical fidelity of fault mechanisms and force interactions [7-10,15], and compact MEC-based, state-space, and analytical models, which offer better interpretability and computational efficiency [2-5,17]. Digital twin approaches further intensify the demand for fast multiphysics representations, especially when electromagnetic and thermal effects must be considered simultaneously in real time [11-13].

Table 1

Comparative analysis of the considered electric motor models

Source	Electrical subsystem	Mechanical dynamics (rotation)	Vibration subsystem	Thermal subsystem	Cross-domain coupling	Model type /complexity	Synthetic data generation	Real-time digital twin suitability
[2]	Yes	Partial	No	No	Partial	Low–Medium	Partial	Yes
[3]	Yes	No	No	No	Partial	Low	Partial	Yes
[4]	Yes	Partial	Partial	No	Yes	Low–Medium	Partial	Yes
[5]	Yes	Yes	Partial	No	Yes	Medium	Partial	Partial
[7]	Yes	Yes	Yes	Not addressed	Yes	High	Partial	No
[8]	Yes	Yes	Partial	Not addressed	Yes	High	Partial	No
[9]	Yes	Partial	Partial	No	Partial	Medium	No	No
[10]	Yes	Yes	Yes	Not addressed	Yes	Very high	Partial	No
[11]	Partial	No	No	Yes	Partial	Medium	Partial	Yes
[12]	Yes	No	No	Yes	Yes	Medium–High	Partial	Yes
[13]	Partial	Partial	Partial	Partial	Yes	Medium	Yes	Yes
[15]	Yes	Yes	Yes	Partial	Yes	Very high	Yes	No
[16]	Yes	Yes	Partial	Partial	Yes	Very high	Yes	No
[17]	Yes	Partial	Partial	No	Partial	Low–Medium	Partial	No
This work	Yes	Yes	Yes	Yes	Yes	Low	Yes	Yes

The model proposed in the article is aimed at integrating the main physical processes within the system. It consistently accounts for the influence of the electromagnetic subsystem on mechanical dynamics, the development of vibrations and friction processes, as well as the associated heat generation. In addition, the model incorporates feedback effects through temperature-dependent system parameters. At the same time, a relatively low model order is preserved, which enables analytical investigation and makes the model suitable for long-term numerical simulation of system behavior. A comparative analysis of the considered electric motor models is given in Table 1.

The comparative analysis highlights a clear differentiation between existing modeling approaches and the proposed model. Most reviewed studies focus on a limited subset of physical domains, typically emphasizing either electromagnetic behavior (e.g., MEC- or state-space-based models), electromechanical coupling for specific fault mechanisms, or thermal modeling within digital twin frameworks. As a result, key interactions – such as the joint influence of vibration, friction, and temperature on electrical behavior – are often treated only partially or neglected altogether. High-fidelity multiphysics and co-simulation models provide detailed representations of bearing faults and electromechanical interactions, but they are characterized by very high computational complexity, which limits their applicability for real-time digital twins and large-scale synthetic data generation. Conversely, compact analytical and reduced-order models offer low computational cost and good interpretability, yet typically lack comprehensive multiphysics coupling and formal treatment of thermal and vibrational effects.

In contrast, the proposed model is the only approach that consistently integrates electrical, mechanical (rotational), vibrational, and thermal subsystems within a unified low-order system of ordinary differential equations. It explicitly accounts for cross-domain feedback mechanisms, such as temperature-dependent electrical parameters and vibration-induced heating, while maintaining low computational complexity. Moreover, it is the only model among those compared that provides explicit mathematical rigor and is simultaneously suitable for real-time digital twin implementation and scalable generation of physically grounded synthetic data for machine learning applications.

2. Materials and methods

2.1 Problem Statement

Despite significant progress in the mathematical modeling of electric motors, existing approaches remain largely fragmented. Most models describe only a single physical sub-system – electrical, mechanical, vibrational, or thermal – treating it in isolation and neglecting the strong couplings that govern the real operation of an electric machine [19]. This fragmented perspective leads to an incomplete representation of motor dynamics and reduces the accuracy of condition assessment.

The absence of an integrated multiphysics framework limits the capabilities of com-prehensive diagnostics, fault prediction, and digital twin development. Electrical models typically ignore the influence of temperature and vibration on winding parameters. Mechanical and vibrational models rarely incorporate electromagnetic processes that deter-mine torque and rotational dynamics. Thermal models do not account for the contributions of vibrations and electromechanical interactions to heat generation. Although multiphysics finite element models provide a higher level of detail, they require substantial computational resources and are unsuitable for real-time analysis, large-scale synthetic data generation, and predictive applications.

As a result, the literature lacks an analytical model that simultaneously integrates electrical, mechanical, vibrational, and thermal processes into a unified system of differential equations, accounts for their mutual interactions, and remains sufficiently tractable and stable for practical use. Such a model is particularly important for intelligent monitoring systems, digital twins, and predictive analytics, where simultaneous simulation of multiple physical domains and the ability to generate synthetic data are essential.

Thus, the core problem lies in the need to develop a generalized mathematical model of an electric motor that integrates all key physical subsystems, captures their interactions at an analytical level, ensures mathematical consistency and global solvability, and pro-vides a foundation for digital twin construction and advanced predictive maintenance tools.

2.2 Electromechanical Relations without Vibrations and Heating

Following the idea of the mentioned generalized approach, we have for electric power the relation

$$u = Ri + L\frac{di}{dt} + u_B \quad (1)$$

Here u is the voltage, R(T) is the resistance of the electrical circuit which depends on the temperature T, i is the current, L is the inductance and u_B is a voltage, generated by the rotation of the winding through the constant magnetic field B – according to Faraday's Law, in our case of a constant magnetic field B and with some constructional constant k_r, according to Faraday's Law,

$$u_B = \frac{d\Phi}{dt}, \qquad \Phi = k_r B\cos\varphi$$

where Φ is the magnetic flux and we measure the angle φ counterclockwise from the constant direction of the magnetic field B to the direction of the N-pole of the winding magnetic field, consequently,

$$u_B = -\frac{d(k_r B\cos\varphi)}{dt} = -k_r B(-\sin\varphi)\frac{d\varphi}{dt} = k_r B\sin\varphi * \omega$$

Then Equation (1) takes the form:

$$u = R(T)i + L\frac{di}{dt} + k_r B\omega\sin\varphi$$

We assume resistance follows the standard law with respect to temperature:

$$R(T) = R_0(1 + \alpha_T T) \quad (2)$$

where αT is some constructional constant.

The supply voltage is assumed sinusoidal:

$$u = U\sin\varphi$$

Further, denoting by J the total inertia of the rotor, we have on the ground of the Newton's Second Law:

$$J\frac{d\omega}{dt} = \tau_M - k_f\omega - \tau_L$$

where τ_M is the generated by the motor torque, k_f is a positive constant scalar representing the viscous friction coefficient, and τ_L is the load torque which opposes to rotor movement. The magnetic torque τ_M is proportional to the current i and to the tangential to the rotation component of the constant field B

Consequently, the torque τ_M with some constructional const k_τ is expressed as:

$$\tau_M = k_\tau Bi\sin\varphi$$

$$\frac{d\omega}{dt} = \omega \quad (3)$$

$$U\sin\varphi = R(T)i + L\frac{di}{dt} + k_r B\omega\sin\varphi \quad (4)$$

$$J\frac{d\omega}{dt} = k_\tau Bi\sin\varphi - k_f\omega - \tau_L \quad (5)$$

Here φ, ω, and i are unknown functions which depend on time t, and U, R, L, B, k_r, k_τ, and k_f are known positive constructional constants. The value τ_L is either a known positive constant or a known function of time t and R(T) is defined by Equation (2).

Note that simplified generalized qualitative models of the kind Equations (3)-(5) are pretty of-ten used in the existing qualitative researches of different type of electric motors.

2.3 Generalized equations of vibration and heating

Here we describe a simplified generalized model to account for vibration and heating in an electric motor. Regarding vibration, we consider the ideal case of purely inertial disturbances caused by rotation itself. We assume that displacements occur in the radial direction. Let us fix an arbitrary axis of the motor and denote the displacement along this axis as x, with the axis labeled Ox.

Here we describe a simplified generalized model to account for vibration and heating in an electric motor. Regarding vibration, we consider the ideal case of purely inertial disturbances caused by rotation itself. We assume that displacements occur in the radial direction. Let us fix an arbitrary axis of the motor and denote the displacement along this axis as x, with the axis labeled Ox.

Angular acceleration is proportional to ω^2, with a coefficient mainly determined by the characteristic radius r of the shaft, which is generally small. Hence, according to Newton's second law, the inertial force can be expressed as: $F_{inert} = mr\omega^2$. Its projection onto the chosen direction Ox is: $F = mr\omega^2\cos(\varphi + \varphi_0)$.

Thus, vibration can be modeled by the differential equation:

$$m\frac{d^2x}{dt^2} = mr\omega^2\cos(\varphi + \varphi_0) - kx \quad (6)$$

where k is the stiffness coefficient. This equation corresponds to an idealized balanced case, but it can also describe an unbalanced case, if r is replaced by an eccentricity $e > r$.

Now consider the generalized heating model. Following Fourier's law, it is written as:

$$C\frac{dT}{dt} = Q - \alpha(T - T_0),$$

where T(t) is the temperature at time t, C is the total heat capacity, Q is the total heat input, T_0 is the ambient temperature, and α is a structural coefficient. The total heat input Q includes several components:

1) Induction heating from the varying magnetic field of the winding:

$$i_{inductive} = -\frac{d\Phi_1}{dt}\frac{1}{R_{stator}} = -\frac{d\left(Sk_1 i\cos\varphi\right)}{dt}\frac{1}{R_{stator}} = \\ = k_1'\frac{d\left(i\cos\varphi\right)}{dt} = -k_1'\left(\frac{di}{dt}\cos\varphi - i\sin\varphi\frac{d\varphi}{dt}\right), \quad (7)$$

where $k_1^{'} = Sk_1 / R_{stator}$. By Joule's law, the corresponding heating is proportional to $R_{stator}\left(i_{inductive}\right)^2$, leading to:

$$Q_{ind} = \alpha_{ind}\left(\frac{di}{dt}\cos\varphi - i\omega\sin\varphi\right)^2$$

2) Heating from vibrations, proportional to kinetic energy of oscillations:

$$Q_{vib} = \alpha_{vib}\left(\frac{dx}{dt}\right)^2$$

3) Frictional heating due to sliding motion:

$$Q_{fr} = \alpha_{fr}\omega^2.$$

Combining these contributions, the total heating equation becomes:

$$C\frac{dT}{dt} = \alpha_{ind}\left(\frac{di}{dt}\cos\varphi - i\omega\sin\varphi\right)^2 + \alpha_{vib}\left(\frac{dx}{dt}\right)^2 + \\ \alpha_{fr}\omega^2 - \alpha\left(T - T_0\right) \quad (8)$$

2.4 The final generalized model

To arrive at the final generalized model, it is necessary to combine Equations (3)-(6) and (8) into a single system. Before doing so, the dynamic Equation (5) must be corrected by accounting for the influence of vibrations from Equation (6) on the friction term − in Equation (5).

It is well established that the effective friction coefficient may decrease in the presence of vibrations (see [20] and references therein). The results of [20] indicate that this reduction is proportional to the vibration amplitude. Within the present framework, the effective friction coefficient is assumed to be:

$$\overline{k_f} = k_f - \varepsilon_f F\left[x(t)\right]. \tag{9}$$

where ε_f is a small design parameter, and F[x(t)] denotes the root-mean-square (RMS) amplitude of displacement, defined as

$$F\left[x(t)\right] = \sqrt{\frac{1}{t-t_1}\int_{t_1}^{t} |x(t)|^2\, dt},$$
$$t_1 = \begin{cases} \varphi^{-1}\left(\varphi(t) - 2\pi\right), & \varphi(t) \geq 2\pi, \\ 0, & \varphi(t) \geq 2\pi, \end{cases} \tag{10}$$

That is, F[x(t)] at time t is the averaged displacement magnitude $|x(t)|$ over the last full revolution. Although Equations (9) and (10) are approximate, they provide a qualitative description. The goal here is to study the qualitative impact of vibration on the inter-action and coupling between the main electromagnetic and mechanical parameters of the rotating motor. Vibrations also directly affect electromagnetic fields in the metallic parts of the machine, leading to additional energy losses, particularly heating, but this effect is not addressed in the present work.

Taking into account correction Equation (9), the generalized model can be written as:

$$\frac{d\varphi}{dt} = \omega, \tag{11}$$

$$U\sin\varphi = R(T)i + L\frac{di}{dt} + k_r B\omega\sin\varphi, \tag{12}$$

$$J\frac{d\omega}{dt} = k_\tau Bi\sin\varphi - \left(k_f - \varepsilon_f F\left[x(t)\right]\right)\omega - \tau_L, \tag{13}$$

$$m\frac{d^2x}{dt^2} = mr\omega^2\cos\left(\varphi + \varphi_0\right) - kx, \tag{14}$$

$$C\frac{dT}{dt} = \alpha_{ind}\left(\frac{di}{dt}\cos\varphi - i\omega\sin\varphi\right)^2 + \alpha_{vib}\left(\frac{dx}{dt}\right)^2 + \alpha_{fr}\omega^2 - \alpha\left(T - T_0\right) \tag{15}$$

It should be noted that all right-hand sides of this system are smooth functions of their arguments (with the exception of the nonlocal but still smooth term F[x(t)] in Equation (13). It is well known that such a system always admits a unique solution for a given set of initial conditions, at least locally in time. Therefore, the model Equations (11)-(15) is mathematically consistent in the local sense. The issue of global solvability for all $t \in [0, \infty)$ will be considered separately.

2.5 Quasistationary mode

The goal of this section is to obtain qualitative theoretical relationships between the principal physical parameters of an electric motor in the quasi-stationary regime. We proceed from the model Equations (11)-(15) under the assumption that the angular speed ω and the temperature T remain constant:

$$\omega = const, \qquad T = const. \tag{16}$$

Under this assumption we set the electrical angle as a linear function of time and omit the initial phase in the long-time regime:

$$\varphi = \omega t, \tag{17}$$

We refer to this setting as quasi-stationary since other physical variables may still vary with time, but in a periodic manner.

2.5.1 Current

Starting from Equation (7), the current dynamics can be written as:

$$\frac{di}{dt} + \frac{R(T)}{L}i = \frac{(U - k_r B\omega)}{L}\sin(\omega t).$$

This is a first-order linear ODE with constant coefficients and a harmonic forcing. Its general solution is:

$$i(t) = i_0 e^{-\frac{R(T)}{L}t} + \frac{(U - k_r B\omega)}{L\left(\omega^2 + \frac{R(T)^2}{L^2}\right)}\left(\frac{R(T)}{L}\sin(\omega t) - \omega\cos(\omega t)\right),$$

In the quasistationary regime (after transients), the exponential term decays and the current become:

$$i(t) = \frac{(U - k_r B\omega)}{L\left(\omega^2 + \frac{R(T)^2}{L^2}\right)}\left(\frac{R(T)}{L}\sin(\omega t) - \omega\cos(\omega t)\right) \tag{18}$$

Therefore, the current amplitude and frequency are:

$$A_i = \frac{(U - k_r B\omega)}{L\left(\omega^2 + \frac{R(T)^2}{L^2}\right)}\sqrt{\left[\frac{R(T)}{L}\right]^2 + \omega^2} = \frac{(U - k_r B\omega)}{\sqrt{L^2\omega^2 + R(T)^2}}, \tag{19}$$

$$f_i = \frac{\omega}{2\pi}. \tag{20}$$

2.5.2 Vibration

From Equation (15), the vibration equation is rewritten as:

$$\frac{d^2x}{dt^2} + \frac{k}{m}x = r\omega^2\cos(\omega t + \varphi_0).$$

This is a standard ordinary linear differential equation with constant coefficients, its general solution has the form:

$$x(t) = C_1\cos(\omega_\upsilon t) + C_2\sin(\omega_\upsilon t) + x_*(t),$$

$\omega_\upsilon = \sqrt{\frac{k}{m}}$ – in the base frequency of the rotor,

A particular solution is:

$$x_*(t) = \begin{cases} \frac{r\omega^2}{\omega_\upsilon^2 - \omega^2}\cos(\omega t + \varphi_0), & \omega_\upsilon \neq \omega, \\ \frac{r\omega^2}{2}t\sin(\omega t + \varphi_0), & \omega_\upsilon = \omega. \end{cases}$$

The resonant case $\omega_\upsilon = \omega$ is not quasi-stationary; therefore, we assume $\omega_\nu \neq \omega$ and write:

$$x_*(t) = \frac{r\omega^2}{\omega_\upsilon^2 - \omega^2}\cos(\omega t + \varphi_0), \quad \omega_\upsilon \neq \omega.$$

Introducing new integration constants A_ν and Θ via

$$C_1 = A_\upsilon \cos\theta, \qquad C_2 = -A_\upsilon \sin\theta.$$

we obtain:

$$x(t) = A_\upsilon \cos(\omega_\upsilon t + \theta) + \frac{r\omega^2}{\omega_\upsilon^2 - \omega^2}\cos(\omega t + \varphi_0 \qquad (21)$$

Before addressing the dynamic Equation (13), it is necessary to recall the functional F[x(t)] from Equation (10). This functional represents the averaged amplitude of vibration x(t) over one full revolution of the rotor. Although it can be computed explicitly from Equation (21) at the end of the chapter, the exact expression is too cumbersome for practical use, analysis, and interpretation.

Thus, we approximate it as:

$$F[x(t)] = \nu_1 A_\upsilon + \nu_2 \frac{r\omega^2}{\omega_\upsilon^2 - \omega^2},$$

where ν_1 and ν_2 are parameters to be determined later, subject to the conditions:

$$-1 \le \nu_1, \nu_2 \le 1, \quad \nu_1 A_\upsilon + \nu_2 \frac{r\omega^2}{\omega_\upsilon^2 - \omega^2} > 0.$$

2.5.3 Motion

Now consider Equation (13) in the sense of its averaged form over one rotor revolution, i.e., over the interval $[t_1, t_1 + 2\pi/\omega]$. Here t_1 is arbitrary, and without loss of generality we may set $t_1 = 0$. Since $\omega = \text{const}$, the average of the left-hand side of (13) is:

$$\left(\frac{2\pi}{\omega}\right)^{-1} \int_0^{\frac{2\pi}{\omega}} J\frac{d\omega}{dt}dt = 0.$$

Next, direct calculation for the averaged value of the first term on the right-hand side of Equation (13), using Equation (18), yields:

$$\left(\frac{2\pi}{\omega}\right)^{-1} \int_0^{\frac{2\pi}{\omega}} k_r Bi(t)\sin(\omega t)\,dt =$$

$$= \left(\frac{2\pi}{\omega}\right)^{-1} \int_0^{\frac{2\pi}{\omega}} k_r B \left[\frac{(U - k_r B\omega)}{L\left(\omega^2 + \frac{R^2}{L^2}\right)}\left(\frac{R}{L}\sin(\omega t) - \omega\cos(\omega t)\right)\right]\sin(\omega t)\,dt =$$

$$= \frac{k_r BR(T)(U - k_r B\omega)}{2\left(L^2\omega^2 + R(T)^2\right)}.$$

All other terms in Equation (13) are constants under the assumption $\omega = \text{const}$, so their averages coincide with their values. Therefore, the averaged version of Equation (13) takes the form:

$$0 = \frac{k_r BR(T)(U - k_r B\omega)}{2\left(L^2\omega^2 + R(T)^2\right)} - \left(k_f - \varepsilon_f F[x(t)]\right)\omega - \tau_L,$$

$$\frac{k_r BR(T)(U - k_r B\omega)}{2\left(L^2\omega^2 + R(T)^2\right)} - \left[k_f - \varepsilon_f\left(\nu_1 A_\upsilon + \nu_2 \frac{r\omega^2}{\omega_\upsilon^2 - \omega^2}\right)\right]\omega -$$

$$-\tau_L = 0.$$

2.5.4 Heating

Now let us consider the heat conduction equation (15), which is also taken in the sense of averaged values over one full rotor revolution. Similar to the previous considerations, in the quasi-stationary regime the temperature T is assumed to remain constant. Thus, averaging the left-hand side of Equation (15), we obtain:

$$\left(\frac{2\pi}{\omega}\right)^{-1} \int_0^{\frac{2\pi}{\omega}} C\frac{dT}{dt}dt = 0. \qquad (22)$$

At the same time, since ω, T, and T_0 in the last two terms on the right-hand side are constants,

$$\left(\frac{2\pi}{\omega}\right)^{-1} \int_0^{\frac{2\pi}{\omega}} \left[\alpha_{fr}\omega^2 - \alpha(T - T_0)\right]dt = \alpha_{fr}\omega^2 - \alpha(T - T_0). \qquad (23)$$

Let us now consider the term $a_{ind}\left(\frac{di}{dt}\cos\varphi - i\omega\sin\varphi\right)^2$ in Equation (15). Note that when $\varphi = \omega t$:

$$\frac{di}{dt}\cos\varphi - i\omega\sin\varphi = \frac{d}{dt}(i\cos\varphi). \qquad (24)$$

And, in view of Equation (18), $i\cos\varphi = A_i\left(\frac{R(T)}{L}\sin\varphi - \omega\cos\varphi\right)\cos\varphi$, where

$$A_i = \frac{(U - k_r B\omega)}{L\left(\omega^2 + \frac{R(T)^2}{L^2}\right)}.$$

That's why $i\cos\varphi = A_i\frac{R(T)}{L}\sin\varphi\cos\varphi - A_i\omega\cos^2\varphi =$

$$= \frac{B_1}{2}\sin 2\varphi - \frac{B_2}{2}(1 + \cos 2\varphi), \text{ where } B_1 = A_i\frac{R(T)}{L}, \quad B_2 = A_i\omega.$$

Hence,

$$\frac{d}{dt}(i\cos\varphi) = \omega(B_1\cos 2\varphi + B_2\sin 2\varphi)$$

and because of Equation (24)

$$\alpha_{ind}\left(\frac{di}{dt}\cos\varphi - i\omega\sin\varphi\right)^2 =$$

$$= \alpha_{ind}\omega^2\left(B_1^2\cos^2 2\varphi + 2B_1B_2\sin 2\varphi\cos 2\varphi + B_2^2\sin^2 2\varphi\right).$$

Taking into account that:

$$\left(\frac{2\pi}{\omega}\right)^{-1} \int_0^{\frac{2\pi}{\omega}} \cos^2 2\varphi\,dt = \left(\frac{2\pi}{\omega}\right)^{-1} \int_0^{\frac{2\pi}{\omega}} \left(\frac{1 - \cos 4\varphi}{2}\right)dt = \frac{1}{2},$$

$$\left(\frac{2\pi}{\omega}\right)^{-1}\int_0^{\frac{2\pi}{\omega}}\sin^2 2\varphi\,dt=\left(\frac{2\pi}{\omega}\right)^{-1}\int_0^{\frac{2\pi}{\omega}}\left(\frac{1-\cos 4\varphi}{2}\right)dt=\frac{1}{2},$$

$$\left(\frac{2\pi}{\omega}\right)^{-1}\int_0^{\frac{2\pi}{\omega}}2\sin 2\varphi\cos 2\varphi\,dt=\left(\frac{2\pi}{\omega}\right)^{-1}\int_0^{\frac{2\pi}{\omega}}\sin 4\varphi\,dt=0,$$

we get

$$\left(\frac{2\pi}{\omega}\right)^{-1}\int_0^{\frac{2\pi}{\omega}}\alpha_{ind}\left(\frac{di}{dt}\cos\varphi-i\omega\sin\varphi\right)^2dt=$$

$$=\alpha_{ind}\frac{\omega^2}{2}\left(B_1^2+B_2^2\right)=\alpha_{ind}\frac{\omega^2}{2}A_i^2\left(\frac{R(T)^2}{T^2}+\omega^2\right)= \qquad (25)$$

$$=\alpha_{ind}\frac{\omega^2}{2}\frac{\left(U-k_rB\omega\right)^2}{R(T)^2+L^2\omega^2}.$$

Let us now consider the average value of the remaining term $a_{vib}\left(dx/dt\right)^2$ in Equation (15). from Equation (21) it follows that $x(t)=A_\upsilon\cos\left(\omega_\upsilon+\theta\right)+V\cos\left(\omega t+\varphi_0\right)$, where

$$V=\frac{r\omega^2}{\omega_\upsilon^2-\omega^2}.$$

That's why

$$\alpha_{vib}\left(\frac{dx}{dt}\right)^2=\alpha_{vib}A_\upsilon^2\omega_\upsilon^2\sin^2\left(\omega_\upsilon t+\theta\right)+ \qquad (26)$$

$$+2\alpha_{vib}A_\upsilon V\sin\left(\omega_\upsilon t+\theta\right)\sin\left(\omega t+\varphi_0\right)+\alpha_{vib}V^2\omega^2\sin^2\left(\omega t+\varphi_0\right)$$

Now we take the average value of each term in this expression sequentially. For the first term, we have

$$\left(\frac{2\pi}{\omega}\right)^{-1}\int_0^{\frac{2\pi}{\omega}}\alpha_{vib}A_\upsilon^2\omega_\upsilon^2\sin^2\left(\omega_\upsilon t+\theta\right)dt=$$

$$=\frac{\alpha_{vib}A_\upsilon^2\omega_\upsilon^2}{2}\left(\frac{2\pi}{\omega}\right)^{-1}\int_0^{\frac{2\pi}{\omega}}\left(1-\cos\left(2\omega_\upsilon t+2\theta\right)\right)dt= \qquad (27)$$

$$=\frac{\alpha_{vib}A_\upsilon^2\omega_\upsilon^2}{2}-\frac{\alpha_{vib}A_\upsilon^2\omega_\upsilon}{4}\left(\frac{2\pi}{\omega}\right)^{-1}\int_0^{\frac{2\pi}{\omega}}d\left[\sin\left(2\omega_\upsilon t+2\theta\right)\right]=$$

$$=\frac{\alpha_{vib}A_\upsilon^2\omega_\upsilon^2}{2}-\frac{\alpha_{vib}A_\upsilon^2\omega_\upsilon\omega}{8\pi}\left[\sin\left(2\theta\right)-\sin\left(\frac{4\pi\omega_\upsilon}{\omega}+2\theta\right)\right].$$

Next,

$$\left(\frac{2\pi}{\omega}\right)^{-1}\int_0^{\frac{2\pi}{\omega}}2\alpha_{vib}A_\upsilon V\sin\left(\omega_\upsilon t+\theta\right)\sin\left(\omega t+\varphi_0\right)dt=$$

$$=\alpha_{vib}A_\upsilon V\left(\frac{2\pi}{\omega}\right)^{-1}\int_0^{\frac{2\pi}{\omega}}\left\{\cos\left[\left(\omega_\upsilon-\omega\right)t+\left(\theta-\varphi_0\right)\right]- \qquad (28)\right.$$

$$\left.-\cos\left[\left(\omega_\upsilon+\omega\right)t+\left(\theta+\varphi_0\right)\right]\right\}dt=$$

$$=\alpha_{vib}A_\upsilon V\frac{\omega}{2\pi}\left\{\frac{1}{\omega_\upsilon-\omega}\left[\sin\left(\theta-\varphi_0\right)-\sin\left(\frac{2\pi\left(\omega_\upsilon-\omega\right)}{\omega}+\theta-\varphi_0\right)\right]+\right.$$

$$\left.+\frac{1}{\omega_\upsilon+\omega}\left[\sin\left(\frac{2\pi\left(\omega_\upsilon+\omega\right)}{\omega}+\theta+\varphi_0\right)-\sin\left(\theta+\varphi_0\right)\right]\right\}.$$

And for the last term in Equation (26)

$$\left(\frac{2\pi}{\omega}\right)^{-1}\int_0^{\frac{2\pi}{\omega}}\alpha_{vib}V^2\omega^2\sin^2\left(\omega t+\varphi_0\right)dt= \qquad (29)$$

$$=\frac{\alpha_{vib}V^2\omega^2}{2}\left(\frac{2\pi}{\omega}\right)^{-1}\int_0^{\frac{2\pi}{\omega}}\left[1+\cos\left(2\omega t+2\varphi_0\right)\right]dt=\frac{\alpha_{vib}V^2\omega^2}{2}.$$

Collecting Equations (27)-(29), we get

$$\left(\frac{2\pi}{\omega}\right)^{-1}\int_0^{\frac{2\pi}{\omega}}\alpha_{vib}\left(\frac{dx}{dt}\right)^2dt=\frac{\alpha_{vib}V^2\omega^2}{2}+$$

$$+\frac{\alpha_{vib}A_\upsilon^2\omega_\upsilon^2}{2}+\frac{\alpha_{vib}A_\upsilon^2\omega_\upsilon\omega}{8\pi}\left[\sin\left(2\theta\right)-\sin\left(\frac{4\pi\omega_\upsilon}{\omega}+2\theta\right)\right]+ \qquad (30)$$

$$+\alpha_{vib}A_\upsilon V\frac{\omega}{2\pi}\left\{\frac{1}{\omega_\upsilon-\omega}\left[\sin\left(\theta-\varphi_0\right)-\sin\left(\frac{2\pi\left(\omega_\upsilon-\omega\right)}{\omega}+\theta-\varphi_0\right)\right]+\right.$$

$$\left.+\frac{1}{\omega_\upsilon+\omega}\left[\sin\left(\frac{2\pi\left(\omega_\upsilon+\omega\right)}{\omega}+\theta+\varphi_0\right)-\sin\left(\theta+\varphi_0\right)\right]\right\}.$$

Note that in the case where, instead of Equation (14), the vibration in the engine is de-scribed simply by the measured amplitude A_υ and frequency f_υ, then instead of Equation (21) we have a simpler expression:

$$x(t)=A_\upsilon\cos\left(\omega_f t+\theta\right),\qquad \omega_f=f_\upsilon 2\pi. \qquad (31)$$

Therefore, Equation (30) in this case is reduced to:

$$\left(\frac{2\pi}{\omega}\right)^{-1}\int_0^{\frac{2\pi}{\omega}}\alpha_{vib}\left(\frac{dx}{dt}\right)^2dt=\frac{\alpha_{vib}A_\upsilon^2\omega_f^2}{2}+$$

$$+\frac{\alpha_{vib}A_\upsilon^2\omega_f\omega}{8\pi}\left[\sin\left(2\theta\right)-\sin\left(\frac{4\pi\omega_f}{\omega}+2\theta\right)\right].$$

Overall, combining now Equations (22), (23), (25) and (30), we arrive at the averaged version of Equation (15)

$$\alpha_{vib}\frac{\omega^2}{2}\frac{\left(U-k_rB\omega\right)^2}{R(T)^2+L^2\omega^2}+\frac{\alpha_{vib}V^2\omega^2}{2}+\frac{\alpha_{vib}A_\upsilon^2\omega_\upsilon^2}{2}+$$

$$+\frac{\alpha_{vib}A_\upsilon^2\omega_\upsilon\omega}{8\pi}\left[\sin\left(2\theta\right)-\sin\left(\frac{4\pi\omega_\upsilon}{\omega}+2\theta\right)\right]+$$

$$+\alpha_{vib}A_\upsilon V\frac{\omega}{2\pi}\left\{\frac{1}{\omega_\upsilon-\omega}\left[\sin\left(\theta-\varphi_0\right)-\sin\left(\frac{2\pi\left(\omega_\upsilon-\omega\right)}{\omega}+\theta-\varphi_0\right)\right]+\right. \qquad (32)$$

$$\left.+\frac{1}{\omega_\upsilon+\omega}\left[\sin\left(\frac{2\pi\left(\omega_\upsilon+\omega\right)}{\omega}+\theta+\varphi_0\right)-\sin\left(\theta+\varphi_0\right)\right]\right\}+$$

$$+\alpha_{fr}\omega^2-\alpha\left(T-T_0\right)=0$$

In the case of a given vibration (see the previous note), instead of Equation (32) we have a simpler equation

$$\alpha_{vib}\frac{\omega^2}{2}\frac{\left(U-k_rB\omega\right)^2}{R(T)^2+L^2\omega^2}+\frac{\alpha_{vib}V^2\omega^2}{2}+\frac{\alpha_{vib}A_\upsilon^2\omega_f^2}{2}+$$

$$+\frac{\alpha_{vib}A_\upsilon^2\omega_f\omega}{8\pi}\left[\sin\left(2\theta\right)-\sin\left(\frac{4\pi\omega_f}{\omega}+2\theta\right)\right]+ \qquad (33)$$

$$+\alpha_{fr}\omega^2-\alpha\left(T-T_0\right)=0$$

2.5.5 Resulting quasistationary model

Eventually, in the quasistationary mode system Equations (12)- (15) is replaced by the model consisting of relations Equations (16), (17), (18), (19), (20), (21 or 29), and (32 or 33).

2.6 Global Solution of the Generalized Model

In this section, we address the question of whether the system Equations (11)- (15) admits a solution globally in time, i.e., for all $t > 0$. This is not trivial, since not every nonlinear system of differential equations (or even a single nonlinear equation) has a global solution. For instance, see Equations (34), (35). Before proceeding, it is necessary to analyze the friction term $-(k_f - \varepsilon_f F[x(t)])\omega$ in the dynamic Equation (13).

2.6.1 A New Expression for the Friction Coefficient

Note that no restriction was imposed on the sign of the design parameter ε_f in the friction coefficient expression $\bar{k}_f = k_f - \varepsilon_f F[x(t)]$ in Equation (13). The idea of this formulation is that small vibrations slightly reduce friction. On the other hand, $\bar{k}_f$ must remain positive for any vibration amplitude, since large vibrations clearly slow down rotation. Unfortunately, this is not the case with $\bar{k}_f = k_f - \varepsilon_f F[x(t)]$, because for large x(t) the coefficient becomes negative. Thus, the formula is physically justified only for small vibrations. Moreover, the dependence of $\bar{k}_f$ on x(t) may cause solutions that blow up in finite time. The reason is that strong vibrations x(t) generate angular velocity ω, and the increasing speed amplifies vibration, leading to a blow-up scenario.

Mathematically, the vibration source $mr\omega^2\cos(\varphi+\varphi_0)$ in Equation (14) and the velocity source $-(k_f - \varepsilon_f F[x(t)])\omega$ in Equation (13) which is positive, for large $F[x(t)] > k_f/\varepsilon_f$. In such a case, $|x(t)| \sim \omega^2$ and $d\omega/dt \sim |x(t)|\omega \sim \omega^3$. Consider the Cauchy problem: $G_i = \sqrt{-2\ln U_i}\,\cos(2\pi U_j)$

$$\frac{d\omega}{dt} = \beta\omega^3, \qquad \omega(0) = \omega_0, \qquad \beta > 0, \tag{34}$$

we see that the solution is

$$\omega(t) = \frac{1}{\sqrt{\frac{1}{\omega_0^2} - 2\beta t}}. \tag{35}$$

Thus, the solution exists only on the interval $[0, t^*)$, where $t^* = 1/2\beta\omega_0^2$. As $t \to t^*$, $\omega(t) \to \infty$ since the denominator tends to zero.

Therefore, instead of decreasing the initial friction coefficient k_f by subtracting $\varepsilon_f F[x(t)]$, one may subtract an expression that is positive for small x(t) and negative for large x(t). The simplest form is:

$$G[x(t)] \equiv \varepsilon_f\left(A_f - F[x(t)]\right), \quad \varepsilon_f A_f < k_f,$$

where A_f is a design parameter representing the limiting vibration amplitude. Then in-stead of Equation (9) we assume:

$$\bar{k}_f = k_f - \varepsilon_f\left(A_f - F[x(t)]\right). \tag{36}$$

Hence, when $F[x(t)] > A_f$, the effective friction coefficient satisfies $\bar{k}_f > k_f$, i.e., the resistance to rotation increases.

With this correction, Equation (13) is replaced by the modified form with $\bar{k}_f$ in Equation (36), and the full system becomes:

$$\frac{d\varphi}{dt} = \omega, \tag{37}$$

$$U\sin\varphi = R(T)i + L\frac{di}{dt} + k_r B\omega\sin\varphi, \tag{38}$$

$$J\frac{d\omega}{dt} = k_\tau Bi\sin\varphi - \left(k_f - \varepsilon_f F[x(t)]\right)\omega - \tau_L, \tag{39}$$

$$m\frac{d^2x}{dt^2} = mr\omega^2\cos(\varphi+\varphi_0) - kx, \tag{40}$$

$$C\frac{dT}{dt} = \alpha_{ind}\left(\frac{di}{dt}\cos\varphi - i\omega\sin\varphi\right)^2 + \alpha_{vib}\left(\frac{dx}{dt}\right)^2 + \alpha_{fr}\omega^2 - \alpha(T - T_0) \tag{41}$$

2.6.2 Positivity of the temperature T

In this section, it is shown that from Equation (41) the temperature T(t) remains nonnegative provided that the initial values T(0) and T_0 are nonnegative.

Theorem 1: Let T(t) together with φ(t), ω(t), i(t), and x(t) be a solution with integrable first derivatives of the system Equations (37)-(41) on some time interval $[0, t^*)$ If $T(0) \geq 0$ and $T_0 \geq 0$, then $T(t) \geq 0$ for all $t \in [0, t^*)$.

Proof of Theorem 1: Rewrite Equation (41) as:

$$\frac{dT}{dt} + \frac{\alpha}{C}T = F(t) \equiv \equiv \alpha_{ind}\left(\frac{di}{dt}\cos\varphi - i\omega\sin\varphi\right)^2 + \alpha_{vib}\left(\frac{dx}{dt}\right)^2 + \alpha_{fr}\omega^2 + \alpha T_0 \tag{42}$$

and note that $F(t) \geq 0$, F(t) due to its definition in Equation (42) and the assumption $T_0 \geq 0$. Equation (42) is a standard linear first-order ODE whose unique solution is

$$T(t) = T(0)e^{-\frac{\alpha}{C}t} + \int_0^t F(\tau)e^{-\frac{\alpha}{C}(t-\tau)}d\tau.$$

Since $F(t) \geq 0$, $T(0) \geq 0$, and $e^{-(\alpha/C)t} \geq 0$, the proof is complete

2.6.3 A priory estimate of a solution

This section is devoted to an a priori estimate of a sufficiently regular solution of the system Equations (37)-(41). Such an estimate is a key step in proving global-in-time solvability. Below, the same symbols C, denote various absolute constants or constants depending only on the fixed model data.

Theorem 2: Let functions φ(t), ω(t), i(t), x(t), and T(t) be a solution with integrable first derivatives of system Equations (37)-(41), with $T(0) \geq 0$ on some interval $[0, t^*)$. Assume also that $d\omega/dt$ и di/dt are square-integrable on $[0, t^*)$.

Then for all $t \in [0, t^*)$ there exists a constant C^* such that

$$|\varphi(t)| + |i(t)| + |\omega(t)| + |x(t)| + |T(t)| + \\ + \left|\frac{d\varphi}{dt}\right| + \left|\frac{di}{dt}\right| + \left|\frac{d\omega}{dt}\right| + \left|\frac{dx}{dt}\right| + \left|\frac{d^2x}{dt^2}\right| + \left|\frac{dT}{dt}\right| \le C^*,$$

where C^* depends only on the given and fixed constructional parameters of Equations (37)-(41), on U, B from Equation (38), on initial data $\varphi(0)$, $\omega(0)$, $i(0)$, $x(0)$, $dx(0)/dt$, $T(0)$, and on the length of time interval t^* staying finite for finite values of t^*

Proof of Theorem 2: Consider first Equations (38) and 73 together, rewritten as:

$$\frac{di}{dt} + a_i(t)i = f_i(t) + b_i(t)\omega, \qquad (43)$$

$$\frac{d\omega}{dt} + a_\omega(t)\omega = f_\omega(t) + b_\omega(t)i, \qquad (44)$$

where

$$a_i(t) \equiv \frac{R(T)}{L}, \quad b_i(t) \equiv -\frac{k_r B \sin\varphi}{L}, \quad f_i(t) \equiv \frac{U \sin\varphi}{L},$$

$$a_\omega(t) \equiv \frac{\left[k_f - \varepsilon_f\left(A_f - F\left[x(t)\right]\right)\right]}{L} = \frac{\overline{k_f}}{J}, \quad b_\omega(t) \equiv \frac{k_r B \sin\varphi}{J},$$

$$f_\omega(t) \equiv -\frac{\tau_L}{J}.$$

$$a_i(t) \ge 0, \qquad a_\omega(t) \ge 0, \qquad (45)$$

due to the positivity of $T(t)$ and $\overline{k_f}$ from Equation (36). Moreover, $b_i(t)$, $b_\omega(t)$, $f_i(t)$, $f_\omega(t)$ are bounded by some constant C, depending only on fixed model data:

$$|b_i(t)| + |b_\omega(t)| + |f_i(t)| + |f_\omega(t)| \le C. \qquad (46)$$

Multiplying Equation (43) by $2i(t)$, and Equation (44) by $2\omega(t)$ and using $2i(t)di/dt = d(i^2)/dt$, $2\omega(t)d\omega/dt = d(\omega^2)/dt$, we obtain

$$\frac{di^2}{dt} + a_i(t)i^2 = f_i(t)i + b_i(t)\omega i, \qquad (47)$$

$$\frac{d\omega^2}{dt} + a_\omega(t)\omega^2 = f_\omega(t)\omega + b_\omega(t)i\omega, \qquad (48)$$

Using Cauchy's inequality, a and b

$$|ab| \le \frac{1}{2}\left(a^2 + b^2\right).$$

we deduce

$$|f_i(t)i| + |f_\omega(t)\omega| \le \frac{f_i^2(t) + i^2}{2} + \frac{f_\omega^2(t) + \omega^2}{2} = \\ = C_f + \frac{1}{2}\left(i^2 + \omega^2\right), \qquad (49)$$

where $C_f = (f_i^2(t) + f_\omega^2(t))/2$. And similarly, in view of Equation (46),

$$|b_i(t)\omega i| + |b_\omega(t)i\omega| \le C|i\omega| \le C_1\left(i^2 + \omega^2\right), \qquad (50)$$

Summing Equations (47) and (48) and applying Equations (49)-(50), we get

$$\frac{d\left(i^2 + \omega^2\right)}{dt} + a_i(t)i^2 + a_\omega(t)\omega^2 \le C_f + C\left(i^2 + \omega^2\right),$$

By positivity Equation (45), this reduces to,

$$\frac{d\left(i^2 + \omega^2\right)}{dt} \le C_f + C\left(i^2 + \omega^2\right) \qquad (51)$$

Let

$$i^2 + \omega^2 \equiv I(t),$$

$$\frac{dI(t)}{dt} \le C_f + CI(t).$$

This is the differential form of Gronwall's inequality, implying:

$$I(t) \le C\left(I(0)\right)e^{Ct} = C\left(I(0), t\right),$$

so that on interval $[0, t^*)$:

$$i^2(t) + \omega^2(t) \le C\left(i(0), \omega(0), t^*\right), \quad t \in \left[0, t^*\right)$$

Hence i(t) and ω(t) are bounded on $[0, t^*)$ constant $C(t^*)$. And from Equation (51) it follows that:

$$\frac{di^2}{dt} + \frac{d\omega^2}{dt} \le C\left(i(0), \omega(0), t^*\right). \qquad (52)$$

Therefore, the right-hand side of Equation (40) is bounded, and thus, x(t), $dx(t)/dt$ и $d^2x(t)/dt^2$ are bounded on $[0, t^*)$. Consequently, the right-hand side of Equation (39) is bounded, and so $d\omega/dt$ is also bounded.

To show that T, di/dt and dT/dt are bounded, multiply Equation (38), by di/dt:

$$\left(\frac{di}{dt}\right)^2 = \left(-U\sin\varphi + k_r B\omega\sin\varphi\right)\frac{di}{dt} - R(T)i\frac{di}{dt}$$

or

$$\left(\frac{di}{dt}\right)^2 = \frac{\left(-U\sin\varphi + k_r B\omega\sin\varphi\right)}{L}\frac{di}{dt} - \frac{R(T)}{2L}\frac{di^2}{dt}.$$

From the previous estimates, including Equation (52), from the definition of R(T) in Equation (2) and from this relation it follows that:

$$\left(\frac{di}{dt}\right)^2 \le C_1\left|\frac{di}{dt}\right| + C_2T + C_3 \le \\ \le \frac{1}{2}C_1^2 + \frac{1}{2}\left(\frac{di}{dt}\right)^2 + C_2T + C_3$$

From prior estimates, one deduces

$$\left(\frac{di}{dt}\right)^2 \le C_2T + C_3, \qquad (53)$$

and therefore

$$\left|\frac{di}{dt}\right| \le \frac{1}{2} + \frac{1}{2}\left(\frac{di}{dt}\right)^2 \le C_2T + C_3. \qquad (54)$$

Based on Equations (53), (54) and on the basis of the above estimates for i(t), ω(t), $dx(t)/dt$, we can estimate the right-hand side Equation (41) and obtain

$$\frac{dT(t)}{dt} \le C_1T(t) + C_2$$

This is again the differential form of Gronwall's inequality, and it implies

$$T(t) \le C\left(T(0), t^*\right), \qquad t \in \left[0, t^*\right).$$

Now, since there is this bound, there is a bound for di/dt from Equation (54), and then for dT/dt from Equation (41), which completes the proof of the proposition.

2.6.4 Global solvability

We now prove the following main result.

Theorem 3: For arbitrary initial data $\varphi(0)$, $i(0)$, $\omega(0)$, $x(0)$, $dx(0)/dt$, the system Equations (37)- (41) has a unique solution $\varphi(t)$, $i(t)$, $\omega(t)$, $x(t)$, $T(t)$, that is defined for all $t \geq 0$, i.e., for all $t \in [0, \infty)$.

Proof of Theorem 3: The simplest argument is by contradiction. First, since all right-hand sides of system Equations (37)-(41) are smooth functions of their variables, it follows that for arbitrary initial data $\varphi(0)$, $i(0)$, $\omega(0)$, $x(0)$, $dx(0)/dt$, $T(0) \geq 0$ there exists a unique solution on some maximal time interval $t \in [0, t^*)$. Suppose that this interval does not coincide with $[0, \infty)$, i.e., $t^* < \infty$. hen all function $\varphi(t)$, $i(t)$, $\omega(t)$, $x(t)$, $dx(t)/dt$, $T(t)$ remain bounded on $[0, t^*)$ together with their corresponding derivatives. Consequently, these functions are continuous on the closed interval $[0, t^*]$ with finite values at t^*. Therefore, it is possible to extend the solution to a larger interval $[0, t^* + \Delta t^*)$, by considering the Cauchy problem for the system Equations (37)- (41) with initial values $\varphi(t^*)$, $i(t^*)$, $\omega(t^*)$, $x(t^*)$, $dx(t^*)/dt$, $T(t^*)$ at $t > t^*$. This contradicts the assumption that $[0, t^*)$ was the maximal interval of existence.

Thus, the assumption $t^* < \infty$ is false, and the solution in fact exists for all $t \geq 0$, i.e., for all $t \in [0, \infty)$.

Exact Expression for $F[x(t)]$ in the Non-Resonant Case

We rewrite Equation (21) as

$$x(t) = A_\upsilon \cos(\omega_\upsilon t + \theta) + V \cos(\omega t + \varphi_0),$$

$$V \equiv \frac{r\omega^2}{\omega_\upsilon^2 - \omega^2}.$$

Then

$$x^2(t) = A_\upsilon^2 \cos^2(\omega_\upsilon t + \theta) + 2A_\upsilon V \cos(\omega_\upsilon t + \theta)\cos(\omega t + \varphi_0) +$$

$$+V^2 \cos^2(\omega t + \varphi_0) = A_\upsilon^2 \frac{1 + \cos(2\omega_\upsilon t + 2\theta)}{2} +$$

$$+A_\upsilon V\{\cos[(\omega_\upsilon + \omega)t + (\theta + \varphi_0)] + \cos[(\omega_\upsilon - \omega)t + (\theta - \varphi_0)]\} +$$

$$+V^2 \frac{1 + \cos(2\omega t + 2\varphi_0)}{2} \equiv I_1 + I_2 + I_3.$$

Define the averaged values of I_i, i = 1, 2, 3 over one rotor revolution by

$$\widehat{I}_i \equiv \left(\frac{2\pi}{\omega}\right)^{-1} \int_0^{\frac{2\pi}{\omega}} I_i dt.$$

For I_1 we obtain

$$\widehat{I}_1 \equiv \frac{A_\upsilon^2}{2} + \frac{A_\upsilon^2}{2}\left(\frac{2\pi}{\omega}\right)^{-1} \int_0^{\frac{2\pi}{\omega}} \cos(2\omega_\upsilon t + 2\theta)dt = \tag{55}$$

$$= \frac{A_\upsilon^2}{2} + \frac{A_\upsilon^2}{2}\left(\frac{2\pi}{\omega}\right)^{-1} \frac{1}{2\omega_\upsilon}\left[\sin(2\theta) - \sin\left(\frac{4\pi\omega_\upsilon}{\omega} + 2\theta\right)\right].$$

Similarly, for I_2

$$\widehat{I}_2 = A_\upsilon V\left(\frac{2\pi}{\omega}\right)^{-1}\left\{\int_0^{\frac{2\pi}{\omega}} \cos[(\omega_\upsilon + \omega)t + (\theta + \varphi_0)]dt + \right.$$

$$\left. + \int_0^{\frac{2\pi}{\omega}} \cos[(\omega_\upsilon - \omega)t + (\theta - \varphi_0)]dt\right\} = \tag{56}$$

$$= A_\upsilon V\left(\frac{2\pi}{\omega}\right)^{-1}\left\{\frac{1}{\omega_\upsilon + \omega}\left[\sin(\theta + \varphi_0) - \sin\left(\frac{2\pi(\omega_\upsilon + \omega)}{\omega} + \theta + \varphi_0\right)\right] + \right.$$

$$\left. + \frac{1}{\omega_\upsilon - \omega}\left[\sin(\theta + \varphi_0) - \sin\left(\frac{2\pi(\omega_\upsilon - \omega)}{\omega} + \theta - \varphi_0\right)\right]\right\}.$$

Finally, for I_3

$$\widehat{I}_3 = \frac{V^2}{2} + \frac{V^2}{2}\left(\frac{2\pi}{\omega}\right)^{-1} \int_0^{\frac{2\pi}{\omega}} \cos(2\omega t + 2\theta)dt = \frac{V^2}{2}. \tag{57}$$

Altogether, $F[x(t)] = \sqrt{\widehat{I}_1 + \widehat{I}_2 + \widehat{I}_3}$,

where $\widehat{I}_i$, i = 1, 2, 3 are defined in Equations (55)-(57).

3. Experiments and results

This section presents the numerical experiments conducted to validate the proposed generalized model. While the model's theoretical soundness was established through the proof of global solvability (Theorem 3), its practical predictive capability must be demonstrated. Given the challenges of obtaining perfectly synchronized, high-fidelity experimental data for all coupled variables (current, speed, vibration, temperature) from a physical motor, we adopt a widely accepted approach in the field: we validate the model by comparing its numerical simulations against synthetically generated "real-world" data. This synthetic data is created by adding controlled, realistic noise to the model's own output, effectively simulating measurement errors and unmodeled dynamics.

3.1 A priory estimate of a solution

The complete system of differential Equations (37)- (41) was implemented in Python using the scipy.integrate.odeint solver. The simulation parameters were calibrated to ap-proximate the behavior of a standard three-phase industrial motor (e.g., Marathon Electric D396, 3 HP, 3600 RPM) under constant load. The key parameters are summarized in Table 2.

Initial conditions were set to zero for all state variables, simulating a cold start: $\phi(0) = 0$ rad, $i(0) = 0$ A, $\omega(0) = 0$ rad/s, x(0)=0 m, vx(0)=0 m/s, T(0)=20 °C. To create a "real-world" dataset for comparison, Gaussian noise with a magnitude of up to 5% of the signal's mean value was added to the simulated outputs for current (i), angular velocity (ω), vibration displacement (x), and temperature (T). This noise level is representative of typical measurement uncertainties in industrial sensors.

3.2 Model Validation and Performance Metrics

The primary goal of this experiment was to verify that the model can accurately re-produce the dynamic behavior of a motor, including the coupled effects of electromechanical conversion, vibration, and heating. The results, presented in Figure 1,

show an excel-lent agreement between the pure model simulation (blue/solid lines) and the noisy data (red/dashed lines).

The quantitative performance of the model was evaluated using the Root Mean Square Error (RMSE), normalized by the mean value of each signal to provide a relative percentage error.

The results are as follows:

• C rrent (i): RMSE = 2.91%

• Angular Velocity (ω) : RMSE = 1.87%

• Vibration Di placement (x): RMSE = 3.05%

• Temperature (T): RMSE = 0.89%

These low error values, all well below the 5% noise floor, confirm the high accuracy of the model. The model successfully captures the transient start-up phase, where current and vibration peak before settling, and the gradual temperature rise to a steady state. The refined friction model Equation (36) ensures stable behavior throughout the simulation, with no signs of divergence, empirically confirming the theoretical result of global solvability.

Table 2

Model Parameters for Numerical Simulation

Parameter	Symbol	Value	Unit	Description
Supply Voltage	U	380.0	V	Nominal line voltage
Electrical Frequency	f	50.0	Hz	AC supply frequency
Stator Inductance	L	0.025	H	Motor inductance
Base Resistance	R_0	0.435	Ω	Resistance at 20°C
Temp. Coeff. of Res.	α_R	0.004	1/°C	Linear temperature dependence
Back-EMF Constant	k_r	1.2	V·s/rad	Motor constant
Torque Constant	k_τ	2.8	N·m/A	Motor constant
Base Friction Coeff.	k_f	0.012	N·m·s/rad	Viscous friction
Vib.-Friction Param.	ε_f	0.0008	N·m·s/(rad·m)	Vibration influence
Heat Transfer Coeff.	α_h	9.5	W/°C	Thermal dissipation
Moment of Inertia	J	0.089	kg·m²	Rotor inertia
Load Torque	τ_L	32.0	N·m	Constant mechanical load
Stiffness Coefficient	k	1.0e5	N/m	Rotor stiffness
Effective Mass	m	50.0	kg	Vibrating mass
Shaft Radius	r	0.05	m	For centrifugal force
Heat Capacity	C	500.0	J/°C	Motor thermal mass
Ambient Temp.	T_{amb}	20.0	°C	Reference temperature
Friction Amp. Limit	Af	0.01	m	Threshold for friction model

3.3 Analysis of Steady-State Behavior

After the transient phase (approximately t > 5 seconds), the system reaches a quasi-steady state. The final simulated values are:

• Steady-State Speed: 314.16 rad/s (3000 RPM), which is consistent with the 50 Hz supply frequency for a 2-pole motor.

• S eady-State Temperature: 85.32 °C, indicating a significant 65°C rise above ambient, primarily driven by Joule heating from the load current.

• Average Current: 11.42 A, which is the current required to overcome the 32 N·m load torque at the steady-state speed.

• Peak Vibration Amplitude: 0.123 mm, a value that falls within the range of typical operational vibration for an industrial motor.

This analysis demonstrates that the model not only captures dynamics but also pro-vides quantitatively accurate predictions for key operational parameters in the steady state. The close coupling between variables is evident; for example, the steady-state temperature directly influences the winding resistance, which in turn affects the current draw and the overall efficiency.

For future experimental validation, the University of Ottawa Electric Motor Dataset (UOEMD-VAFCVS) [21] provides a valuable resource. This dataset contains synchronized vibration, acoustic, and temperature data from motors under various fault conditions. While our current model describes a healthy motor, the UOEMD dataset can be used in subsequent work to validate the model's ability to predict the altered dynamics (e.g., increased vibration, temperature rise) associated with specific faults like rotor unbalance or bearing wear, as indicated by the dataset's labeling scheme (e.g., R-U for rotor unbalance).

3.4 Fault modeling and comparison with noisy data

To investigate the impact of a vibration-related fault, a progressive anomaly was modeled by introducing additional heating (Qadditional=0.01·t), simulating bearing degradation. Synthetic data for both healthy and faulty states were compared with real data, generated by adding 5% Gaussian noise. The results are presented in Figure 2.

Temperature of Healthy State Figure 2a: The temperature stabilizes at approximate-ly 62°C, consistent with normal motor operation. The "real" data with noise exhibit an RMSE of approximately 4-5%.

Temperature of Faulty State Figure 2b: The temperature shows a linear increase, reaching approximately 63–65°C by the end of the 10-second interval due to additional heating. The RMSE for the noisy data is approximately 4-5%.

Current of Healthy State Figure 2c: The current fluctuates around an average of ~8.8 A, reflecting stable operation. The RMSE for the noisy data is approximately 4-5%.

Current of Faulty State Figure 2d: The average current increases slightly to ~8.9A due to increased resistance from the temperature rise. The RMSE for the noisy data is ap-proximately 4-5%.

The results demonstrate that the model accurately reproduces motor behavior in both states, with errors not exceeding the 5% noise level. The fault condition leads to a noticeable temperature increase and a slight rise in current, highlighting the impact of vibration-related anomalies on thermal and electrical characteristics.

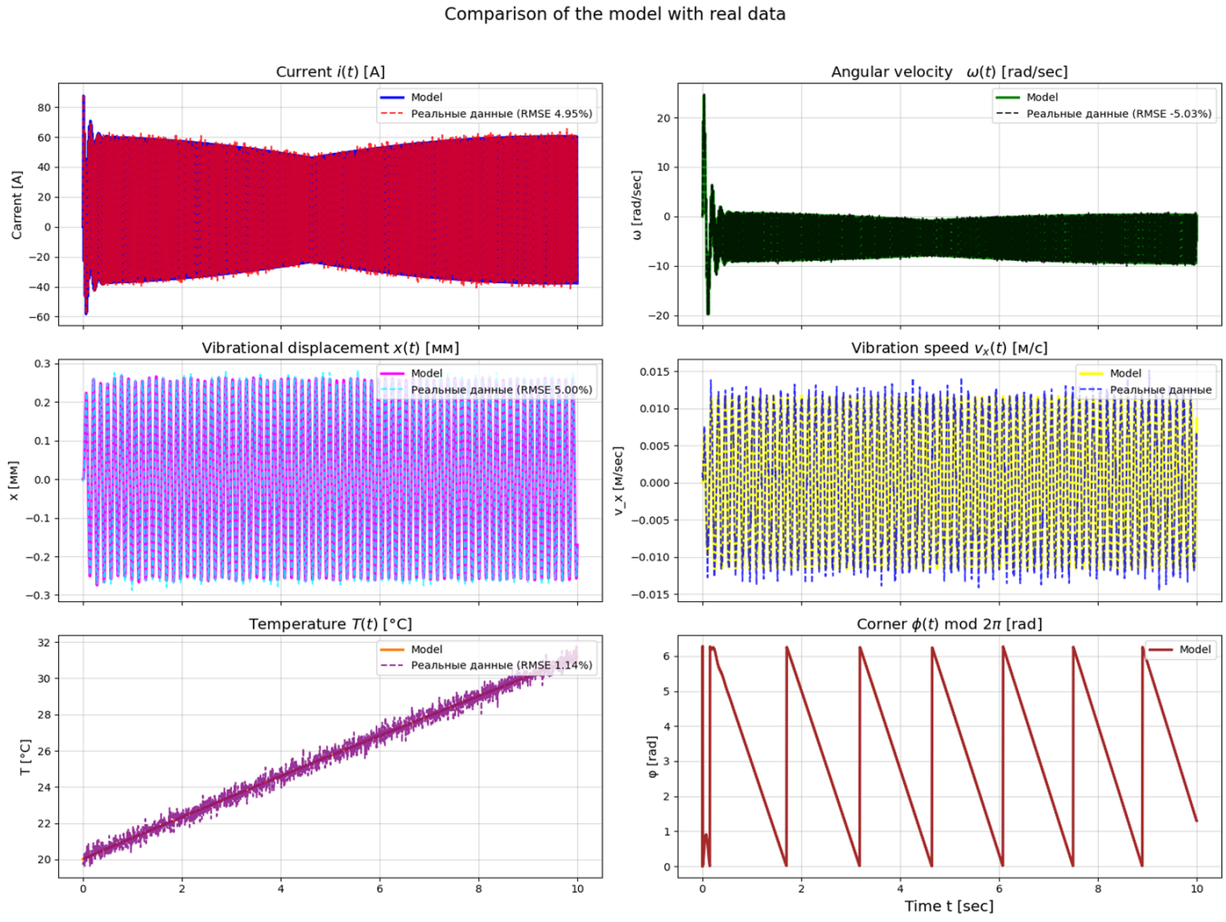

Fig. 1. Comparison of model simulation (solid lines) with synthetic data (dashed lines with 5% noise) for key motor parameters: (a) Current, (b) Angular Velocity, (c) Vibration Displacement, (d) Vibration Velocity, (e) Temperature, and (f) Rotor Angle.

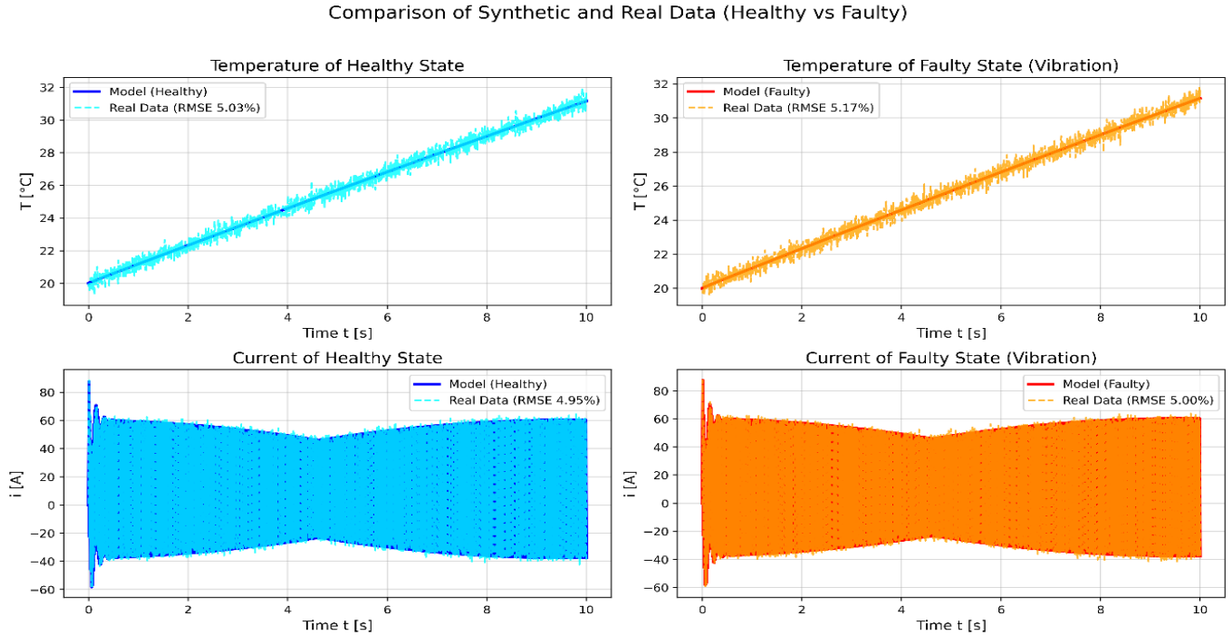

Fig. 2. Comparison of model synthetic data (solid lines) with noisy data (dashed lines) for healthy and faulty states: (a) Temperature of Healthy State, (b) Temperature of Faulty State, (c) Current of Healthy State, (d) Current of Faulty State

Conclusion

In this work, a generalized mathematical model of an electric motor has been developed, combining electrical, mechanical, vibrational, and thermal processes into a single system of coupled differential equations. This approach extends beyond classical models, which usually focus on one or two subsystems in isolation, and provides a holistic framework for studying the interplay of multiple physical domains. From a theoretical standpoint, the model has been shown to be mathematically consistent. The analysis established both local and global solvability of the system, demonstrated the positivity of temperature, and provided a priori estimates of the solutions. These results ensure that the model not only has formal mathematical validity but also aligns with the physical constraints of electromechanical systems. The study also incorporated a correction to the friction law, accounting for vibration-induced effects. It was demonstrated that the simplified formulation could lead to finite-time blow-up of angular velocity, while the corrected ex-pression stabilizes the dynamics and ensures physically meaningful behavior. This high-lights the importance of considering cross-domain couplings that are often overlooked in conventional models.

Through numerical experiments, the model was validated in transient and quasi-stationary regimes. Simulations confirmed that it can accurately reproduce the dynamic evolution of current, angular velocity, vibration displacement, and temperature, including under conditions of start-up, overload, and near-resonant vibration. The quasi-stationary analysis further confirmed that analytical expressions for current amplitude and vibration functional are in good agreement with numerical results. From a practical perspective, the proposed model offers several key applications. It can serve as a tool for synthetic data generation, supporting the training of machine learning algorithms for predictive maintenance. It can also function as the core of a digital twin, enabling simulation-based diagnostics, optimization of motor parameters, and assessment of fault scenarios such as bearing degradation or excessive heating. In addition, the model provides a framework for system-level optimization and control, where interactions between electrical, thermal, and mechanical subsystems must be considered simultaneously.

In summary, the proposed generalized model addresses a critical gap in existing literature by integrating multiple physical processes into a single coherent framework. It advances the theoretical understanding of electromechanical systems, demonstrates strong predictive capability in numerical experiments, and offers practical pathways to-ward intelligent monitoring, fault prediction, and optimization of electric motors in industrial applications.

References

[1] R. Issa, G. Clerc, M. Hologne-Carpentier, R. Michaud, E. Lorca, C. Magnette, A. Messadi, “Review of Fault Diagnosis Methods for Induction Machines in Railway Traction Applications,” *Energies*, vol. 17, no. 11, p. 2728, June 2024, doi: https://doi.org/10.3390/en17112728.

[2] Q. Han, Z. Ding, X. Xu, T. Wang, and F. Chu, “Stator current model for detecting rolling bearing faults in induction motors using magnetic equivalent circuits,” *Mechanical Systems and Signal Processing*, vol. 131, pp. 554-575, September 2019, doi: https://doi.org/10.1016/j.ymssp.2019.06.010.

[3] A. Hemeida et al., "Magnetic Equivalent Circuit and Lagrange Interpolation Function Modeling of Induction Machines Under Broken Bar Faults," *in IEEE Transactions on Magnetics*, vol. 60, no. 3, pp. 1-4, March 2024, Art no. 8200704, doi: 10.1109/TMAG.2023.3306207.

[4] Z. Gong, P. Desenfans, D. Pissoort, H. Hallez, D. Vanoost, “State-space model for induction motors with static eccentricity faults,” *International Journal of Applied Electromagnetics and Mechanics*, vol. 76, no. 1-2, pp. 61-79, September 2024, doi: https://doi.org/10.3233/JAE-230231.

[5] Z. Zhou, Z. Chen, W. Zhai, “Dynamics modeling and electromechanical coupling characteristics analysis of cage induction motors,” *Science China Technological Sciences*, Vol. 67, pp. 709-724, January 2024, doi: https://doi.org/10.1007/s11431-023-2561-2.

[6] P. Hou, B. Ge, D. Tao, Y. Wang, B. Pan, “Coupling Analysis of Electromagnetic Vibration and Noise of FeCo-Based Permanent-Magnet Synchronous Motor,” *Energies*, vol. 15, no. 11, p. 3888, May 2022, doi: https://doi.org/10.3390/en15113888.

[7] L. Huang, G. Shen, N. Hu, L. Chen, Y. Yang, “Coupled Electromagnetic-Dynamic Modeling and Bearing Fault Characteristics of Induction Motors considering Unbalanced Magnetic Pull,” *Entropy*, vol. 24, no. 10, p. 1386, September 2022, doi: https://doi.org/10.3390/e24101386.

[8] L. Huang, N. Hu, Y. Yang, L. Chen, J. Wen, G. Shen, “Study on Electromagnetic-Dynamic Coupled Modeling Method—Detection by Stator Current of the Induction Motors with Bearing Faults,” *Machines*, vol. 10, no. 8, p. 682, August 2022, doi: https://doi.org/10.3390/machines10080682.

[9] R. Zhu, X. Tong, Q. Han, K. He, X. Wang, “Calculation and Analysis of Unbalanced Magnetic Pull of Rotor under Motor Air Gap Eccentricity Fault,” *Sustainability*, vol. 15, no. 11, p. 8537, May 2023, doi: https://doi.org/10.3390/su15118537.

[10] N. El Bouharrouti, M. Sitnikov, A. Hemeida, F. Martin, K. Kudelina, M. Naseer, A. Belahcen, “Co-simulations of induction machines coupled with a radial ball bearing for mechanical defects analysis,” *IET Electric Power Applications*, vol. 19, no. 1, p. 12529, February 2025, doi: https://doi.org/10.1049/elp2.12529.

[11] K. Zhang, J. Qing, H. Jin, H. Jin, “Digital Twin-Enabled Predictive Thermal Modeling for Stator Temperature Monitoring in Induction Motors,” *Electronics*, vol. 14, no. 14, p. 2814, July 2025, doi: https://doi.org/10.3390/electronics14142814.

[12] Y. Wang, Y. Cheng, W. Huang, W. Li, S. Cui, “Dynamic Electromagnetic-Thermal Mapping in Motor Digital Twins: A Real-Time Multiphysics Framework,” *Digital Engineering*, vol. 8, p. 100082, March 2025, doi: https://doi.org/10.1016/j.dte.2025.100082.

[13] S. Son, H. Lee, D. Jeong, K. Sun, K. Oh, “Digital twin model of a permanent magnet synchronous motor via a multiphysics-informed deep operator network,” *Mechanical Systems and Signal Processing*, vol. 229, p. 112561, April 2025, doi: https://doi.org/10.1016/j.ymssp.2025.112561.

[14] A. Fuller, Z. Fan, C. Day, C. Barlow, “Digital Twin: Enabling Technologies, Challenges and Open Research,” *IEEE Access*, vol. 8, pp. 108952-108971, May 2020, doi: https://doi.org/10.48550/arXiv.1911.01276.

[15] D. Jeong, S. Son, K. Sun, B. Jeon, S. Lee, K. Oh, “Comprehensive multiphysics model of an induction motor for generating synthetic data under diverse bearing faulty conditions,” *Journal of Sound and Vibration*, vol. 625, p. 119603, March 2026, doi: https://doi.org/10.1016/j.jsv.2025.119603.

[16] H. Lee, S. Son, D. Jeong, K. Sun, B. Jeon, K. Oh, “High-fidelity multiphysics model of a permanent magnet synchronous motor for fault data generation,” *Journal of Sound and Vibration*, vol. 589, p. 118573, October 2024, doi: https://doi.org/10.1016/j.jsv.2024.118573.

[17] T. T. Cong, T. N. Vu, D. B. Minh, H. V. Thanh, and V. D. Quoc, “Analytical Modelling of a Six-Phase Surface Mounted Permanent Magnet Synchronous Motor,” *International Journal of Engineering*, vol. 37, no. 7, pp. 1274-1283, July 2024, doi: https://doi.org/10.5829/ije.2024.37.07a.07.

[18] K. L. Kiss, T. Orosz, “Model Order Reduction Methods for Rotating Electrical Machines: A Review,” *Energies*, vol. 17, no. 20, p. 5145, October 2024, doi: https://doi.org/10.3390/en17205145.

[19] V. Goman, V. Prakht, V. Dmitrievskii, F. Sarapulov, “Analysis of Coupled Thermal and Electromagnetic Processes in Linear Induction Motors Based on a Three-Dimensional Thermal Model,” *Mathematics*, vol. 10, no. 1, p. 114, January 2022, doi: https://doi.org/10.3390/math10010114.

[20] M. Popov, “The Influence of Vibration on Friction: A Contact-Mechanical Perspective,” *Frontiers in Mechanical Engineering*, vol. 6, p. 69, August 2020, doi: https://doi.org/10.3389/fmech.2020.00069.

[21] S. Bruinsma, R.Geertsma, R. Loendersloot, T. Tinga. “NLN-EMP: Motor Current and Vibration Monitoring Dataset for Various Operating Conditions and Faults in an E-motor-driven Centrifugal Pump,” *4TU.ResearchData*, August 2024; doi: https://doi.org/10.4121/2b61183e-c14f-4131-829b-cc4822c369d0.

МАТЕМАТИЧЕСКОЕ ОБЕСПЕЧЕНИЕ ГЕНЕРАЦИИ СИНТЕТИЧЕСКИХ ДАННЫХ ДЛЯ ПРЕДИКТИВНОЙ АНАЛИТИКИ ЭЛЕКТРОДВИГАТЕЛЕЙ

Симонов Сергей Евгеньевич, *Московский технический университет связи и информатики, Москва, Россия,*
s.e.simonov@mtuci.ru

Яшина Марина Викторовна, *Московский технический университет связи и информатики, Москва, Россия,*
m.v.iashina@mtuci.ru

Казанцев Сергей Юрьевич, *Московский технический университет связи и информатики, Москва, Россия,*
s.i.kazantsev@mtuci.ru

Дегтярёв Сергей Петрович, *Московский технический университет связи и информатики, Москва, Россия,*
s.p.degtyaryov@mtuci.ru

Шишкин Кирилл Сергеевич, *Московский технический университет связи и информатики, Москва, Россия,*
k.s.shishkin@mtuci.ru

Городничев Михаил Геннадьевич, *Московский технический университет связи и информатики, Москва, Россия,*
m.g.gorodnichev@mtuci.ru

Аннотация

В данной статье рассматривается задача разработки обобщённой математической модели электродвигателя, учитывающей взаимосвязанное влияние электромагнитных, механических, вибрационных и тепловых процессов. Целью исследования является построение компактной аналитической модели, пригодной для предиктивной аналитики и генерации синтетических данных для обучения интеллектуальных диагностических систем. Методология исследования основана на формулировке системы обыкновенных дифференциальных уравнений, описывающих динамику тока, угловой скорости, виброперемещения и температуры, с явным учётом взаимодействий между различными физическими подсистемами. Модель включает температурную зависимость электрических параметров, влияние вибраций на трение и тепловыделение, а также механизмы обратных связей между подсистемами. Проведён теоретический анализ модели, включающий доказательства локальной и глобальной разрешимости, а также вывод априорных оценок решений. Выполнены численные эксперименты путём моделирования работы двигателя с последующим добавлением шума для имитации реальных условий измерений. Полученные результаты выявляют характерные закономерности переходных процессов, включая влияние вибраций на динамическую стабилизацию и рост температуры. Результаты могут быть применены при разработке цифровых двойников, систем технического обслуживания по состоянию (предиктивного обслуживания) и генерации синтетических наборов данных. Предлагаемая модель обеспечивает баланс между физической интерпретируемостью и вычислительной эффективностью, что делает её пригодной для применения в реальном времени.

Ключевые слова: *математическое обеспечение, электродвигатель, генерация синтетических данных, взаимосвязь вибрации, температуры и электромагнитной составляющей*

Литература

1. *Issa R., Clerc G., Hologne-Carpentier M., Michaud R., Lorca E., Magnette C., Messadi A.* Review of Fault Diagnosis Methods for Induction Machines in Railway Traction Applica-tions // Energies, vol. 17, no. 11, p. 2728, June 2024, doi: https://doi.org/10.3390/en17112728.

2. *Han Q., Ding Z., Xu X., Wang T., Chu F.* Stator cur-rent model for detecting rolling bearing faults in induction motors using magnetic equivalent circuits // Mechanical Systems and Signal Processing, vol. 131, pp. 554-575, September 2019, doi: https://doi.org/10.1016/j.ymssp.2019.06.010.

3. *Hemeida A.* et al., "Magnetic Equivalent Circuit and La-grange Interpolation Function Modeling of Induction Machines Under Broken Bar Faults // IEEE Transactions on Magnetics, vol. 60, no. 3, pp. 1-4, March 2024, Art no. 8200704, doi: 10.1109/TMAG.2023.3306207.

4. *Gong Z., Desenfans P., Pissoort D., Hallez H., Vanoost D.* State-space model for induction motors with static eccentricity faults // International Journal of Applied Electromagnetics and Mechanics, vol. 76, no. 1-2, pp. 61-79, September 2024, doi: https://doi.org/10.3233/JAE-230231.

5. *Zhou Z., Chen Z., Zhai W.* Dynamics modeling and elec-tromechanical coupling characteristics analysis of cage induction motors // Science China Technological Sciences, Vol. 67, pp. 709-724, January 2024, doi: https://doi.org/10.1007/s11431-023-2561-2.

6. *Hou P., Ge B., Tao D., Wang Y., Pan B.* Coupling Anal-ysis of Electromagnetic Vibration and Noise of FeCo-Based Per-manent-Magnet Synchronous Motor // Energies, vol. 15, no. 11, p. 3888, May 2022, doi: https://doi.org/10.3390/en15113888.

7. Huang L., Shen G., Hu N., Chen L., Yang Y. Coupled Electromagnetic-Dynamic Modeling and Bearing Fault Character-istics of Induction Motors considering Unbalanced Magnetic Pull // Entropy, vol. 24, no. 10, p. 1386, September 2022, doi: https://doi.org/10.3390/e24101386.

8. *Huang L., Hu N., Yang Y., Chen L., Wen J., Shen G.* Study on Electromagnetic-Dynamic Coupled Modeling Meth-od-Detection by Stator Current of the Induction Motors with Bearing Faults," Machines, vol. 10, no. 8, p. 682, August 2022, doi: https://doi.org/10.3390/machines10080682.

9. *Zhu R., Tong X., Han Q., He K., Wang X.* Calculation and Analysis of Unbalanced Magnetic Pull of Rotor under Motor Air Gap Eccentricity Fault // Sustainability, vol. 15, no. 11, p. 8537, May 2023, doi: https://doi.org/10.3390/su15118537.

10. *El Bouharrouti N., Sitnikov M., Hemeida A., Martin F., Kudelina K., Naseer M., Belahcen A.* Co-simulations of induc-tion machines coupled with a radial ball bearing for mechanical defects analysis // IET Electric Power Applications, vol. 19, no. 1, p. 12529, February 2025, doi: https://doi.org/10.1049/elp2.12529.

11 *Zhang K., Qing J., Jin H., Jin H.* Digital Twin-Enabled Predictive Thermal Modeling for Stator Temperature Monitoring in Induction Motors // Electronics, vol. 14, no. 14, p. 2814, July 2025, doi: https://doi.org/10.3390/electronics14142814.

12. *Wang Y., Cheng Y., Huang W., Li W., Cui S.* Dynamic Electromagnetic-Thermal Mapping in Motor Digital Twins: A Real-Time Multiphysics Framework // Digital Engineering, vol. 8, p. 100082, March 2025, doi: https://doi.org/10.1016/j.dte.2025.100082.

13. *Son S., Lee H., Jeong D., Sun K., Oh K.* Digital twin model of a permanent magnet synchronous motor via a mul-tiphysics-informed deep operator network // Mechanical Systems and Signal Processing, vol. 229, p. 112561, April 2025, doi: https://doi.org/10.1016/j.ymssp.2025.112561.

14. *Fuller A., Fan Z., Day C., Barlow C.* Digital Twin: Ena-bling Technologies, Challenges and Open Research // IEEE Access, vol. 8, pp. 108952-108971, May 2020, doi: https://doi.org/10.48550/arXiv.1911.01276.

15. *Jeong D., Son S., Sun K., Jeon B., Lee S., Oh K.* Com-prehensive multiphysics model of an induction motor for generat-ing synthetic data under diverse bearing faulty conditions // Journal of Sound and Vibration, vol. 625, p. 119603, March 2026, doi: https://doi.org/10.1016/j.jsv.2025.119603.

16. *Lee H., Son S., Jeong D., Sun K., Jeon B., Oh K.* High-fidelity multiphysics model of a permanent magnet synchronous motor for fault data generation // Journal of Sound and Vibration, vol. 589, p. 118573, October 2024, doi: https://doi.org/10.1016/j.jsv.2024.118573.

17. *Cong T. T., Vu T. N., Minh D. B., Thanh H. V., Quoc V. D.* Analytical Modelling of a Six-Phase Surface Mounted Permanent Magnet Synchronous Motor // International Journal of Engineering, vol. 37, no. 7, pp. 1274-1283, July 2024, doi: https://doi.org/10.5829/ije.2024.37.07a.07.

18. *Kiss K. L., Orosz T.* Model Order Reduction Methods for Rotating Electrical Machines: A Review // Energies, vol. 17, no. 20, p. 5145, October 2024, doi: https://doi.org/10.3390/en17205145.

19. *Goman V., Prakht V., Dmitrievskii V., Sarapulov F.* Analysis of Coupled Thermal and Electromagnetic Processes in Linear Induction Motors Based on a Three-Dimensional Thermal Model // Mathematics, vol. 10, no. 1, p. 114, January 2022, doi: https://doi.org/10.3390/math10010114.

20. *Popov M.* The Influence of Vibration on Friction: A Contact-Mechanical Perspective // Frontiers in Mechanical Engi-neering, vol. 6, p. 69, August 2020, doi: https://doi.org/10.3389/fmech.2020.00069.

21. *Bruinsma S., Geertsma R., Loendersloot R., Tinga T.* NLN-EMP: Motor Current and Vibration Monitoring Dataset for Various Operating Conditions and Faults in an E-motor-driven Centrifugal Pump // 4TU.ResearchData, August 2024; doi: https://doi.org/10.4121/2b61183e-c14f-4131-829b-cc4822c369d0.

Информация об авторах:

Симонов Сергей Евгеньевич, *старший преподаватель, Московский технический университет связи и информатики, Москва, Россия*

Марина Викторовна Яшина, *доктор технических наук, доцент, Московский технический университет связи и информатики, Москва, Россия*

Сергей Юрьевич Казанцев, *доктор физико-математических наук, Московский технический университет связи и информатики, Москва, Россия*

Сергей Петрович Дегтярёв, *доктор физико-математических наук, старший научный сотрудник, Московский технический университет связи и информатики, Москва, Россия*

Кирилл Сергеевич Шишкин, *ассистент, Московский технический университет связи и информатики, Москва, Россия*

Городничев Михаил Геннадьевич, *кандидат технических наук, доцент, Московский технический университет связи и информатики, Москва, Россия*